View metadata, citation and similar papers at core.ac.uk
brought to you by CORE
provided by CERN Document Server

29th International Cosmic Ray Conference Pune (2005) **10**, 255–270

The PAMELA Space Experiment

Mirko Boezio for the PAMELA collaboration
INFN, Structure of Trieste, Via Valerio, 2 I - 34127 Trieste, Italy
Presenter: M. Boezio (Mirko.Boezio@trieste.infn.it)

PAMELA is a satellite-borne experiment that will make long duration measurements of the cosmic radiation over an extended energy range. Specifically, PAMELA will measure the cosmic-ray antiproton and positron spectra over the largest energy range ever achieved and will search for antinuclei with unprecedented sensitivity. Furthermore, it will measure the light nuclear component of cosmic rays and investigate phenomena connected with solar and earth physics. The apparatus consists of: a time of flight system, a magnetic spectrometer, an anticoincidence system, an electromagnetic imaging calorimeter, a shower tail catcher scintillator and a neutron detector.

All detectors have been successfully integrated in the PAMELA apparatus that has been installed on-board the polar orbiting Resurs DK1 satellite. Beginning of 2006 it will be launched from the Baikonur cosmodrome in Kazakhstan, for a 3 year long mission.

1. Introduction

The PAMELA apparatus (a Payload for Antimatter Matter Exploration and Light-nuclei Astrophysics) is a satellite-borne experiment designed to study charged particles in the cosmic radiation. It will reside in a pressurized vessel attached to a Russian earth-observation satellite, the Resurs DK1, that will be launched into space by a Soyuz TM2 rocket in beginning of 2006 from the Baikonur cosmodrome, in Kazakhstan. The orbit will be elliptical and semi-polar, with an inclination of 70.4° and an altitude varying between 350 km and 600 km. The mission will last at least three years, during which time PAMELA will measure the cosmic-ray composition and energy spectrum.

Table 1. PAMELA Capabilities

Cosmic-ray particle	Energy range
Antiprotons	80 MeV - 190 GeV
Positrons	50 MeV - 270 GeV
Electrons	50 MeV - 800 GeV
Protons	50 MeV - 1 TeV
Electrons+Positrons	up to 2 TeV
Light nuclei (up to Z=6)	100 MeV/n - 500 GeV/n
Light isotopes (D, ^{3}He)	100 MeV/n - 1 GeV/n
Antinuclei	sensitivity better than 10^{-7} in $\overline{\mathrm{He}}$/He up to 70 GeV/n

The PAMELA scientific objectives can be summarized as:

- search for structures in antiparticle spectra;
- search for antinuclei;

- search for antimatter;
- search for dark matter;
- study the cosmic-ray propagation;
- study solar physics and solar modulation;
- study the electron spectrum and investigate the contribution of local sources.

Table 1 shows the various cosmic-ray components and energy ranges over which PAMELA will provide new results.

Antiparticle measurements are the main scientific goals of this experiment. The precise determination of the antiproton and positron spectra will provide important information concerning cosmic-ray propagation and solar modulation. For example, indications of charge dependent solar modulation effects have been already seen in the antiproton to proton ratio data (see [1]).

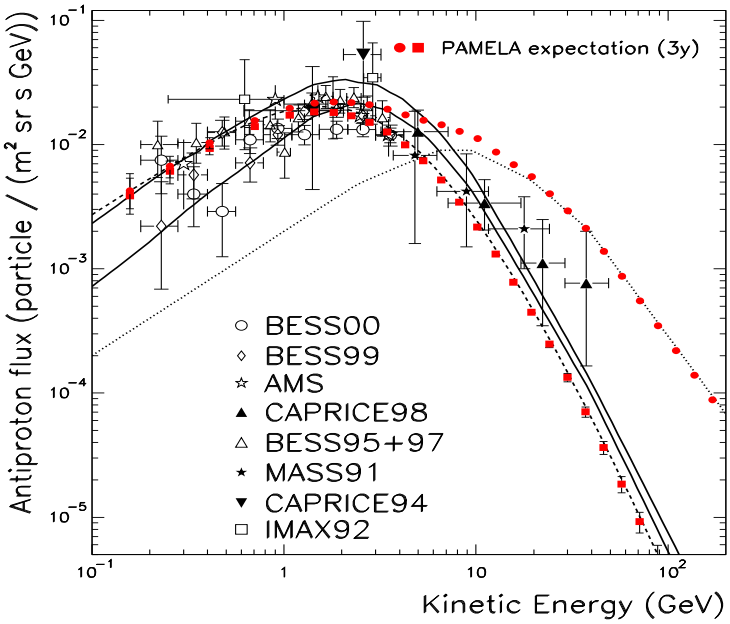

Figure 1. Several recent experimental $\overline{p}$ spectra (BESS00 and BESS99 [1], AMS [6], CAPRICE98 [7], BESS95+97 [8], MASS91 [9], CAPRICE94 [10], IMAX92 [11]) along with theoretical calculations for pure $\overline{p}$ secondary production (solid lines: [12], dashed line: [13]) and for pure $\overline{p}$ primary production (dotted line: [14]). The expected PAMELA performance, in case of a pure secondary component (full boxes) and of an additional primary component (bullets), are indicated. Only statistical errors are included in the expected PAMELA data.

Furthermore, antiparticles can provide hints of new physics since they can be produced from exotic sources such as: primordial black holes (e.g. see [2]), annihilation of supersymmetric particles (e.g. see [3]) or Kaluza-Klein particles (e.g. see [4, 5]).

Figures 1 and 2 show the current status of the cosmic-ray antiproton and positron measurements, respectively, along with some theoretical calculations for pure secondary antiproton and positron production ([12, 13, 25, 26]) and for pure primary antiproton and positron production due to annihilation of supersymmetric particles ([14, 27]). Almost all data available so far have been obtained by balloon-borne experiments. The short data-taking time (approximately 24 hours) and the presence of a residual overburden of atmosphere above the detecting apparatus at the altitudes that a balloon can reach (around 40 km, $\sim$5 g/cm^2 of residual atmosphere) are the main limits of such kinds of measurements. PAMELA will be able to perform very precise measurements with high statistics ($\sim 10^4$ $\overline{\mathrm{p}}$ and $\sim 10^5$ e^+ per year) and over a wider range of energy than ever reached before. The full boxes in figures 1 and 2 indicate the expected PAMELA performance in case of a pure sec-

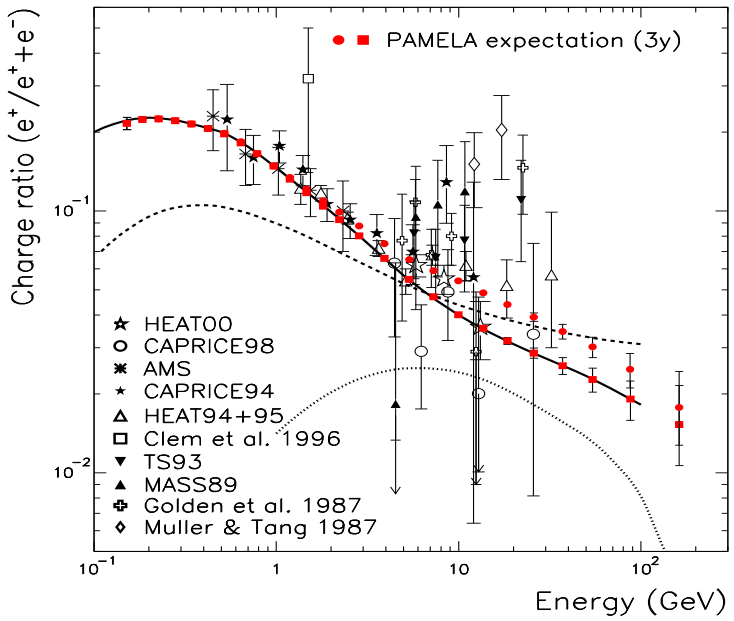

Figure 2. The positron fraction as a function of energy measured by several experiments ([15, 16, 17] and MASS89 [18], TS93 [19], HEAT94+95 [20], CAPRICE94 [21], AMS [22], CAPRICE98 [23], HEAT00 [24]). The dashed [25] and the solid [26] lines are calculations of the secondary positron fraction. The dotted line is a possible contribution from annihilation of neutralinos of mass 336 GeV [27]. The expected PAMELA performance, for a pure secondary component (full boxes) and of an additional primary component (bullets), are indicated. Only statistical errors are included in the expected PAMELA data.

ondary antiproton and positron components and the bullets the expected performance in case of an additional primary component. The errors of the expected PAMELA data points include only statistical uncertainties. An average PAMELA orbit has been used to estimate the vertical geomagnetic cutoffs and the consequent expected number of antiproton and positron events (see [28]).

Additionally, the quasi-polar orbit and low momentum threshold of PAMELA will allow phenomena connected with solar and earth physics to be investigated (further details in [29]). Furthermore, the self-trigger capability

of the electromagnetic calorimeter will extend the electron ($e^- + e^+$) spectrum measurement up to 2 TeV, thus allowing the contribution of local sources to the cosmic radiation to be investigated (e.g. see [30]).

2. The PAMELA apparatus

The apparatus is composed of the following subdetectors, arranged as in Figure 3, from top to bottom:

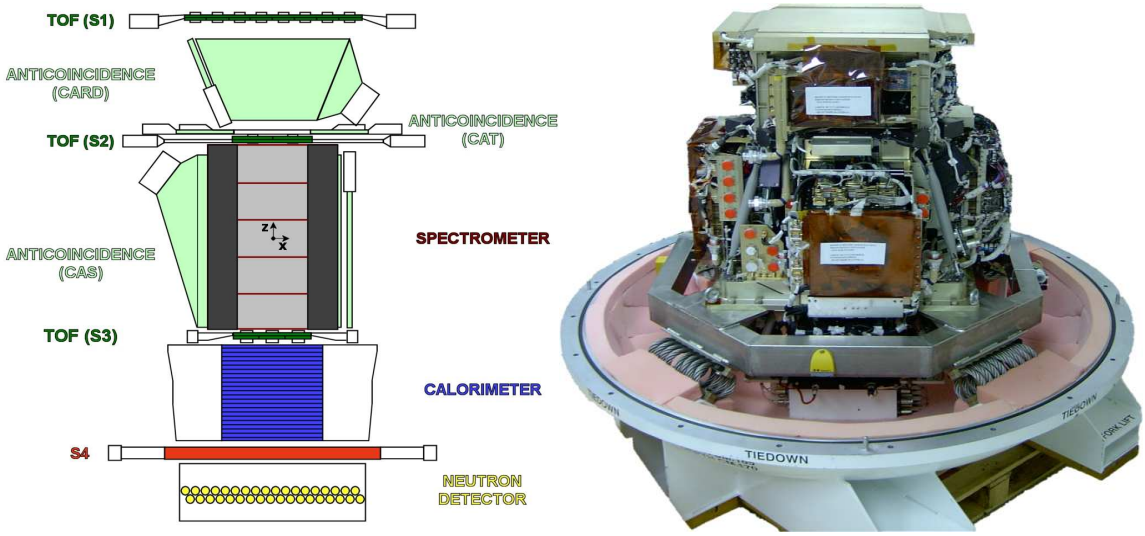

Figure 3. The PAMELA telescope. On the left a sketch of the apparatus and on the right a photo taken just prior delivery to Russia. The detector is approximately 120 cm tall, has a mass of about 450 kg and the power consumption is 360 W. The magnetic field lines in the spectrometer are oriented along the y direction.

- a time of flight system (TOF: S1,S2,S3);
- a magnetic spectrometer;
- an anticoincidence system (CARD, CAT, CAS);
- an electromagnetic imaging calorimeter;
- a shower tail catcher scintillator (S4);
- a neutron detector.

The detector is approximately 120 cm high, has a mass of about 450 kg and the power consumption is 360 W.

2.1 The time of flight system

The ToF system [31] is made of 6 layers of fast plastic scintillators (Bicron BC-404) arranged in three planes (S1, S2 and S3, see figure 3), with alternate layers placed orthogonal to each other.

The sensitive area of each of the two layers of S1 is 330x408 mm^2, the first layer is divided into 8 strips while the second layer is divided into 6 strips. The sensitive area of the S2 and S3 planes is 150x180 mm^2 segmented respectively into 2 by 2 and 3 by 3 strips. The thickness of the S1 and S3 layers is 7 mm while the layers of S2 are only 5 mm thick. The total number of scintillator paddles is 24. Both ends of each scintillator paddle are glued to a one-piece light guide. This is in turn mechanically coupled to a PMT by means of optical pads. Scintillators and light-guides are wrapped in a 25 μm thick Mylar foil. The S3 plane is housed directly in the base plate of PAMELA and kept in place by a set of steel frames. The other two planes are enclosed in light-proof boxes suspended off the PAMELA structure.

The readout electronics of the ToF system is composed of nine boards. Six boards perform the time and charge digitization of the 48 PMT pulses of the PAMELA ToF. Data from these are collected by a DSP board through serial links and, after digital processing, transferred to the main data acquisition system.

A "trigger" board processes the trigger signals [32] from the 48 PMTs of the ToF system and additional ones from other subsystems (S4 and calorimeter) able to generate self-triggers for particular events. About 60 rate counters, dead/live time counters and the logic to generate calibration pulse sequences for different subsystems of the apparatus are also implemented on the board. The logic is distributed on 9 Actel 54SX32A FPGAs. Control masks select trigger types and allows failed (noisy or dead) ToF channels to be vetoed and for each trigger the information on the PMT hit pattern is recorded. A DSP (ADSP 2187L) is used to manage the data structure organization and to monitor the rate counters of the ToF channels and other subsystems.

The combination of the signals from layers of each plane will provide the main trigger of the experiment. The segmentation of each plane in two layers will give redundant information allowing to study the trigger efficiency. Moreover, the ToF system will measure the flight time crossing its planes, thus allowing down-going particles to be separated from up-going ones, and the absolute value of the particles charge Z.

Additional information concerning the ToF system can be found in [33].

2.2 Anticounter System

The PAMELA experiment contains two anticoincidence systems [34] built from plastic scintillators and read out by photomultiplier tubes. Simulations have shown that the majority ($\sim$ 75%) of triggers in space are expected to be false triggers [35], i.e. where the coincidental energy deposits in the time of flight scintillators are generated by secondary particles, produced in the mechanical structure of the experiment. The aim of the anticoincidence systems is to identify these events during offline data analysis. Furthermore, a second level trigger [36] based on information both from the AC detectors and from the calorimeter will provide an online identification of false triggers. This system will be able to reduce the data downloaded to Earth by 60%. These cases are exemplified by figure 4, which shows simulated interactions of cosmic-ray proton with the apparatus. On the left a typical goo trigger event is shown, a false trigger in the centre and on the right a good trigger accompanied by backscattering from the calorimeter in the anticoincidence system. The second level trigger can be enabled via a dedicated command uplinked from ground.

The main AC system [37] consists of 4 plastic scintillators (CAS, see figure 3) surrounding the sides of the magnet and one covering the top (CAT). The second AC system consists of 4 scintillators (CARD) covering the sides of the volume between the first two time-of-flight planes. Each scintillator (Bicron BC-448M) is coupled via a 7 mm thick optical pad to 2 (8 for CAT) photomultiplier tubes (Hamamatsu R5900 PMT), operated at 800 V and read-out by to 2 independent data acquisition boards, for a total of 24 electronic channels. For each channel binary hit information is generated indicating whether the deposited energy exceeds 0.5 mip. The hit information is recorded in a time window of length 1.28 μs centred on the trigger time. Within this window,

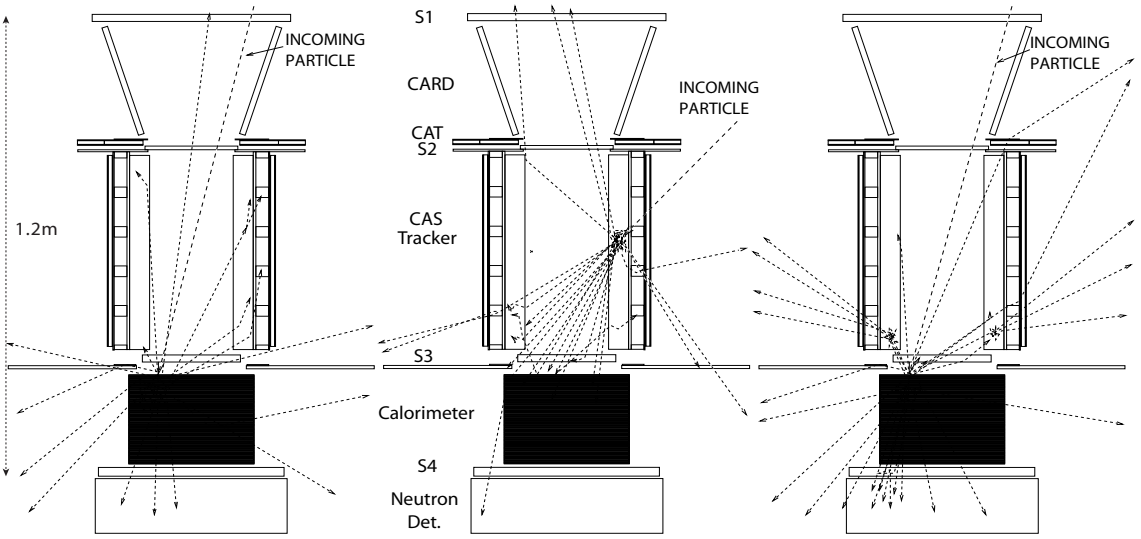

Figure 4. Visual representation of simulated proton interaction in the experiment. (left) Good trigger event without activity in the AC detectors. A particle entering the tracker cavity from the sides may give rise to particle showers that trigger the experiment (false trigger, centre). False trigger events are often characterised by activity in the AC detectors, as are good trigger events with backscattering from the calorimeter (right).

the hit can be located with an accuracy of 80 ns. The in-flight detector performance will be monitored using a LED system.

2.3 Magnetic Spectrometer

The central part of PAMELA apparatus is a magnetic spectrometer [38] consisting of a permanent magnet and a silicon tracker.

The magnet is composed of five modules forming a tower 44.5 cm high. Each module has been built by assembling twelve magnetic blocks, made of a Nd-Fe-B alloy, in a configuration that provides an uniform magnetic field ($\sim$0.43 T) oriented along the y direction (see figure 3) inside a cavity of dimensions 13.2×16.2 cm^{2}sr. The permanent-magnet dimensions define the geometrical factor ($\sim$21.5 cm^2) of the experiment.

Six equidistant detector planes are inserted inside the magnetic cavity. Double sided silicon sensors provide two independent impact coordinates on each plane.

The basic detecting unit is the *ladder*, which is made of two sensors (5.33×7.00 cm^2) assembled with a hybrid circuit that houses the front-end electronics. Each plane is composed by three ladders that are inserted inside an aluminum frame. In order to limit multiple scattering in dead layers, no additional supporting structure is present above or beneath the planes. The strip pitch is 25 μm for the junction side (which is used to measure the coordinate in the bending plane, x view) and one strip out of two is connected to the read–out electronics. On the ohmic side the pitch is 67 μm and strips are orthogonally implanted with respect to the previous ones.

The main task of the spectrometer is to measure the magnetic deflection η of charged particles. Then, the momentum of the particle and the sign of its electric charge are derived from the relation $\eta = Ze/cp$, where e is the electron charge, p the momentum and c the speed of light. The silicon tracking system of the PAMELA

experiment is a powerful instrument, which allows precise determination of particle spectra up to momenta of hundreds of GeV/*c*. Additional information can be found in [39, 40] and references therein.

2.4 Electromagnetic Imaging Calorimeter

This detector is a sampling calorimeter made of silicon sensor planes interleaved with plates of tungsten absorber [41]. Each tungsten layer has a thickness of 0.26 cm, which corresponds to 0.74 X_0 (radiation lengths). Since there are 22 tungsten layers, the total depth is 16.3 X_0 (about 0.6 interaction lengths). Each tungsten plate is sandwiched between two printed circuit boards (called "front-end boards"), which house the silicon detectors and the front-end and ADC electronics. The 380 μm thick silicon detectors developed for the calorimeter are large area devices (8x8 cm^2), segmented into 32 large strips with a pitch of 2.4 mm. In each front-end board the detectors are arranged in a square matrix made by 3×3 devices and each of the 32 strips of a detector is wire-bonded to the corresponding one of the other two detectors in the same row (or column), thus forming 24 cm-long strips. The orientation of the strips of two consecutive layers is shifted by 90°, providing 2-dimensional spatial informations. Figure 5 shows the flight model calorimeter prior delivery to Rome for the

Figure 5. The PAMELA calorimeter flight model.

assembly with the other PAMELA detectors.

One of the main tasks of the calorimeter is to act as a powerful particle identifier to select positrons and antiprotons. In a cosmic-ray experiment like PAMELA, protons and electrons dominate the positive and negative components, respectively, of the cosmic radiation. The longitudinal and transversal segmentation of the calorimeter, combined with the measurement of the particle energy loss in each silicon strip, results in high identification power for electromagnetic showers. Therefore, in the electron and positron analysis, the calorimeter will be used to identify electromagnetic showers whereas in the antiproton analysis it will be used to reject them. The effectiveness of this separation technique is discussed later in the paper.

Additionally, the calorimeter will be used to reconstruct the energy of the electromagnetic showers. This will provide a measurement of the energy of the incident electrons independent from the tracking spectrometer, thus allowing for a cross-calibration of the two energy determinations. The constant term for the calorimeter energy resolution has been estimated as $\sim 5.5\%$ for electromagnetic showers.

2.4.1 *Calorimeter self-trigger*

The calorimeter has been equipped with a "self-trigger" capability, i.e it will generate a trigger signal when a specific energy distribution is detected in predetermined planes of the lower half of the calorimeter[1]. This calorimeter feature will allow PAMELA to measure very high-energy (from $\sim$ 300 GeV to more than 1 TeV) electrons in the cosmic radiation. At present, very few measurements have covered this energy range [42]. Since these events are quite rare in comparison with the "normal" event rate of PAMELA, it is important to have a large geometrical factor in order to increase the statistics during the expected three-year lifetime of the mission. By using the calorimeter to produce the trigger for the apparatus and requiring that the particles enter from one of the first four planes and cross at least 10 radiation lengths, the geometrical factor becomes about 600 cm^2sr, i.e. about a factor of 30 larger than the normal PAMELA acceptance.

The behavior of the calorimeter in self-trigger mode was carefully studied by means of simulations [41]. The simulated energy resolution of the calorimeter in self-trigger mode is fairly constant ($\simeq$ 12%) up to about 800 GeV. At higher energies the resolution decreases because of increasing longitudinal leakage and saturation of the signal from the strips (about 1000 mip).

The choice of energy loss and activated planes implemented in the calorimeter electronics to generate a trigger signal has been taken to have the highest proton rejection while keeping a trigger efficiency of better than 90% for electrons of energies higher than 300 GeV [41]. Combined with the neutron detector information, the apparatus will be able to cleanly identify very high-energy electrons.

2.5 Shower tail catcher scintillator

The detector (S4) is made of a single square scintillator paddle 482×482 mm^2 wide and 10 mm thick read out by six photomultipliers. These are placed three by three on two opposite sides of the scintillator. The detector has an overall efficiency of about $(99.97 \pm 0.02)\%$ and a dynamic range of 1-1000 mip.

The scintillator is located below the calorimeter to detect particles escaping from it and to provide an additional trigger for very high-energy electrons.

2.6 Neutron detector

The purpose of this detector is to complement the electron-proton discrimination capabilities of the PAMELA calorimeter by detecting the much larger neutron production associated with hadronic showers compared to electromagnetic ones in the calorimeter. Furthermore, a joint analysis of the calorimeter and neutron detector information will allow primary electrons to be identified at energies up to 2 TeV.

The neutron detector is made of proportional counters, filled with ^{3}He, surrounded by a polyethylene moderator enveloped in a thin cadmium layer. The 36 counters are stacked in two planes of 18 counters each, oriented along the y-axis of the instrument. The size of the neutron detector is $600 \times 550 \times 150$ mm^3.

[1] The sets of planes used in this configuration can be changed with a dedicated command from ground.

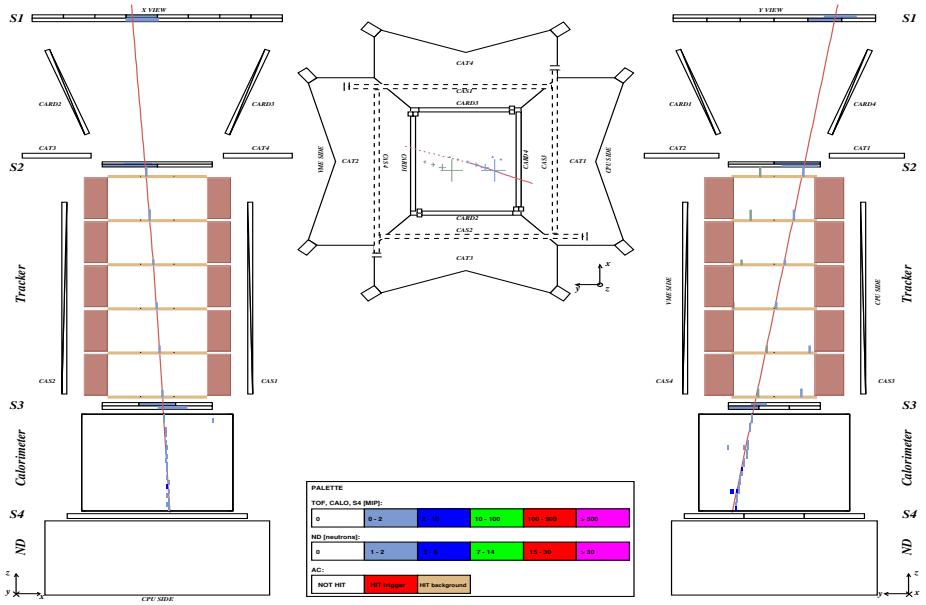

Figure 6. The event display of a 2.8 GeV/c μ^- from ground data in the PAMELA apparatus. On the left the x (bending) and on the right the y view of PAMELA are indicated. In the center PAMELA as seen from above is shown. The signals as detected by PAMELA detectors are shown along with the particle direction (solid lines) reconstructed by the fit procedure of the tracking system data.

3. Data analysis

3.1 Ground data

Prior to the delivery to Russia, the PAMELA apparatus was assembled at the INFN laboratories of Roma II, Rome, Italy. There the system was tested with ground muons over a period of several months. Figures 6 and 7 show two events recorded in Rome. The first is a 2.8 GeV/c negatively charged particle, with high probability of being a μ^- considering the clean non-interacting pattern in the calorimeter. The second is a 66 GeV/c particle with an hadronic interaction in the calorimeter, consistent with a proton. All PAMELA detectors are shown in the figures along with the signals produced by the particles in the detectors and derived information. It can be clearly seen the highly detailed information provided for each cosmic-ray event. The solid lines indicate the tracks reconstructed by the fitting procedure [39] of the tracking system.

From this information the muon charge ratio measured at ground in Rome (50 m a.s.l.) has been obtained and it is presented in Figure 8. Muons were selected as non-interacting particles in the calorimeter and charge one in the ToF scintillators. Additionally low-energy protons were rejected based on the ionization losses in the calorimeter. Their momenta were determined by the tracking system. In the figure PAMELA data are compared with other experimental results [43, 44, 45]. A good agreement can be seen.

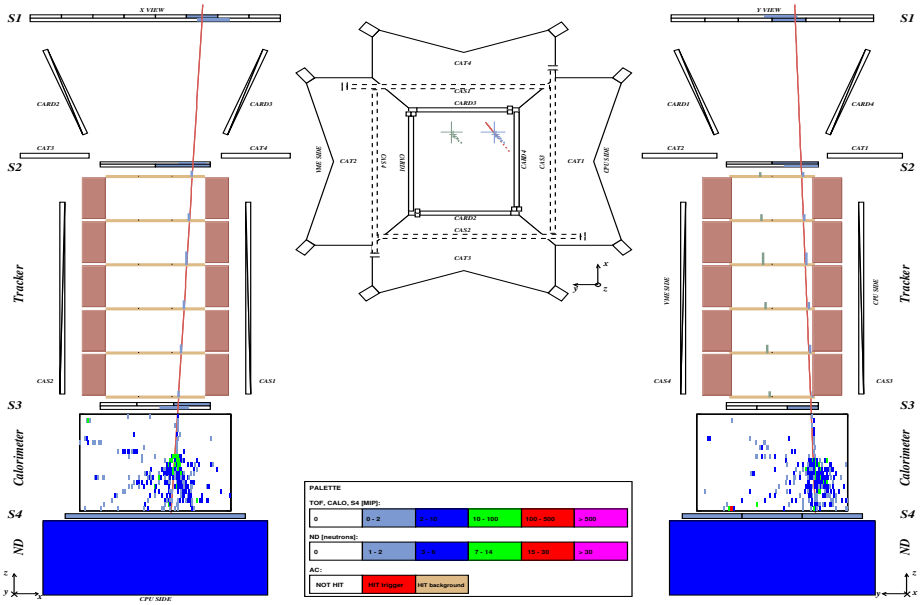

Figure 7. The event display of a 66 GeV/c hadron from ground data in the PAMELA apparatus. On the left the x (bending) and on the right the y view of PAMELA are indicated. In the center PAMELA as seen from above is shown. The signals as detected by PAMELA detectors are shown along with the particle direction (solid lines) reconstructed by the fit procedure of the tracking system data.

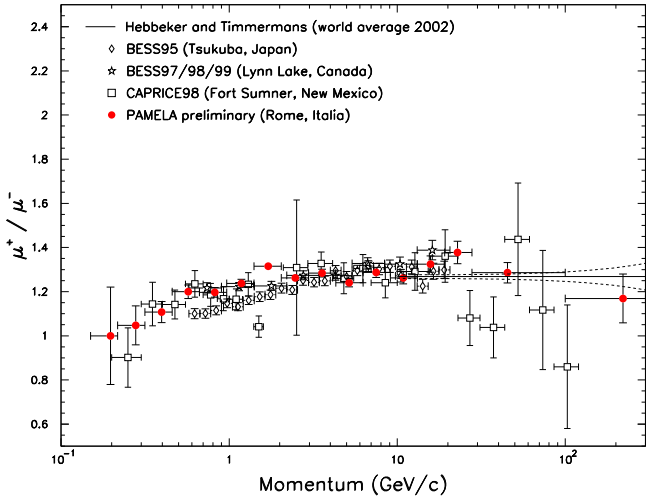

Figure 8. The muon charge ratio at ground measured by PAMELA compared with the 2002 global fit of experimental data by Hebbeker and Timmermans [43] and more recent experimental results [44, 45]. The dashed lines indicate one standard deviation of the fit.

3.2 Flight data

During the flight PAMELA data will be stored onboard the Resurs-DK1 and downlinked to ground at least once per day. The estimated PAMELA data rate is $\sim$ 5 GByte per day. The storage area allocated for PAMELA on the satellite is 20 GByte and the maximum data that will be possible to download to ground in a downlink session is $\sim$ 10 GByte. The main mission control centre will be in Moscow where the first check of the data will be performed. Subsequently, the data will be moved to the various institutions within the PAMELA collaboration.

To realise the scientific goals of the project, it will be necessary to clearly identify the various cosmic-ray components and measure their energy as have been done for the ground data. The separation between down-going and up-going particles, i.e. cosmic rays and albedo particles, will be performed using the ToF information. Figure 9 shows the velocity of the particles (in units of speed of light, β) measured by the ToF system as a

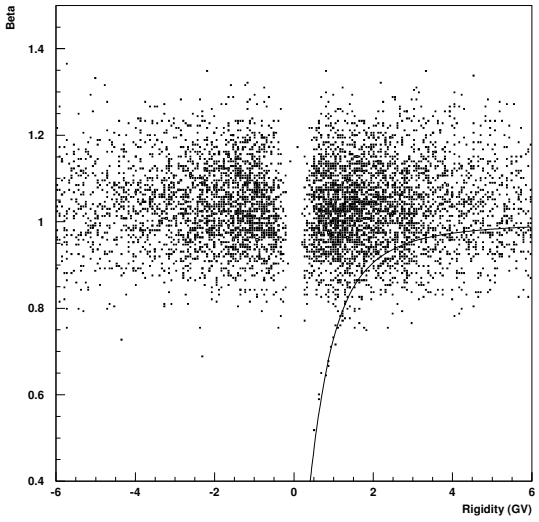

Figure 9. The particle velocity measured by the ToF system as a function of rigidity. The solid line is the theoretical β for protons. The figures comprises about 24000 events from ground data.

function of their rigidity for ground data. Most of the events are relativistic muons with a small proton component visible at low momenta (the solid line indicates the theoretical β for protons). As can be seen in figure 9, the measured time-of-flight resolution of $\simeq$ 300 ps will allow positrons to be separated from protons and antiprotons from electrons up to about 1 GeV/c. Furthermore, the measurement of the ionization losses in the various ToF scintillators will allow the determination of the absolute charge Z of the particles.

The determination of the particle rigidity ($R = 1/\eta$) will be performed by the tracking system. The spatial resolution depends on the particle incidence angle and, in the bending view, is minimal for vertical tracks [40]. For this case beam-test data and simulation studies show a spatial resolution of $\sim 2.8\mu$m and $\sim 13\mu$m, respectively in the bending and non-bending views. Figure 10 shows the resulting deflection error as a function of rigidity obtained with proton beams. From this plot a maximum detectable rigidity (MDR) of $\sim$ 1 TV can

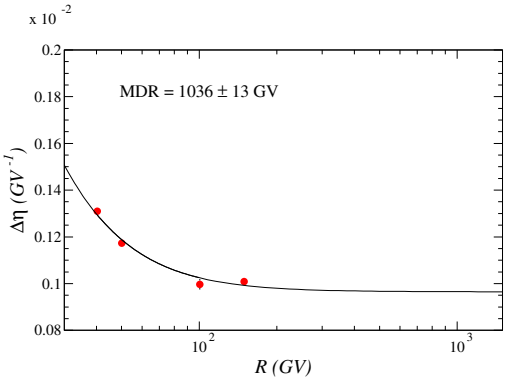

Figure 10. The deflection error measured by the tracking system as a function of rigidity obtained with proton beams.

be inferred. As previously noted, the deflection measurement of the tracking system will be cross-checked with the energy measurement of the calorimeter for high-energy electrons.

The final particle identification will be performed by the calorimeter and neutron detector. The calorimeter hadron/electron separation has been studied using test beam data and simulations. The test beam data used in the analysis were collected at three different occasions at CERN during 2002-2003 both at the PS and SPS beam facilities. A complete description of the calorimeter configuration used in these tests can be found in [28]. The simulations have been performed using variations of the PAMELA Collaboration's official simulation program: GPAMELA [46]. This simulation is based on the GEANT package [47] version 3.21 and uses as default the GEISHA [48] hadron shower Monte Carlo to simulate hadronic interactions.

Figure 11 shows the efficiency (top) and contamination (bottom) of the final electron/positron selection as a function of particle momentum. The full circles represent test beam data and the open squares simulated data. The agreement between simulation and experimental data is reasonable. In the bottom part of figure the proton contamination as function of particle momentum is shown for both test beam data (full circles) as well as for simulated data (open squares). The arrows mark the 68% confidence level when no events survived the selection. The first two data points (at 3 and 10 GeV/c) are for electron/pion separation while the full star and dashed arrow mark the results for simulated protons at 3 and 10 GeV/c respectively. A good agreement between simulation and test beam data also can be seen in this case. These results refer to a partially equipped calorimeter, hence they can be considered as lower limits of the PAMELA calorimeter performances. Additional information can be found in [49].

Antiprotons are identified by selecting electromagnetic showers in the calorimeter with the highest possible efficiency and rejecting them. No test beam data are available for antiprotons and only simulation studies were performed (see [41]).

The neutron detector will add to the calorimeter identification power by separating hadronic from electromagnetic showers [50]. A proton rejection factor of about 10 is expected at 50 GeV and increases with energy. In conclusion the combination of the calorimeter and neutron detector information will provide a proton rejection factor of $\sim 10^6$. Considering that the cosmic-ray proton component increases from about 10^3 times the e^+ component at 1 GeV/c to about 5×10^3 at 10 GeV/c and the cosmic-ray electron component decreases from about 10^3 times the $\overline{p}$ component at 1 GeV/c to less than 10^2 above 10 GeV/c, the proton contamination in the

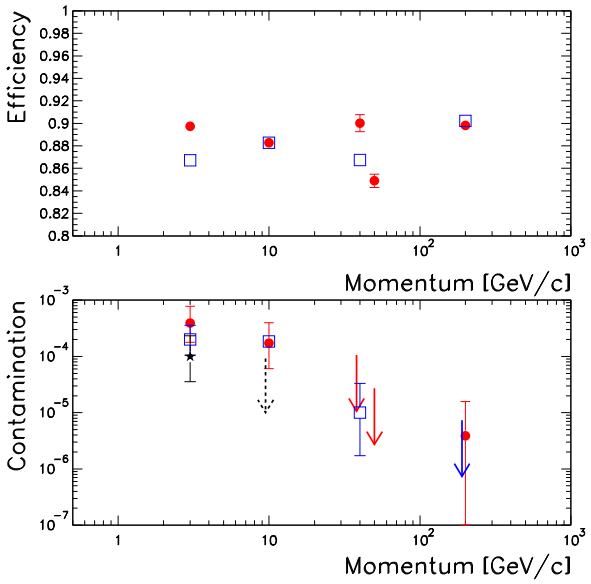

Figure 11. Top: The efficiency for identifying electrons using the electron/positron calorimeter selection as a function of particle momentum. The full circles and open squares represents test beam and simulated data respectively. **Bottom:** The proton contamination of the electron/positron calorimeter selection as a function of particle momentum. The full circles and open squares represent test beam and simulated data respectively, the full triangle is for 3 GeV/c simulated protons, the arrows indicate the 68% confidence level (i.e. no events survived the selection) and the dashed arrow is for simulated protons at 10 GeV/c. The data at 10, 40 and 200 GeV/c are slightly displaced for clarity.

positron sample will be reduced to the percent level and the electron contamination in the antiproton sample to a negligible level.

4. Conclusions

PAMELA is a powerful instrument that will give results of great scientific relevance in several fields of cosmic ray research.

Extensive space qualification tests of PAMELA detectors, electronics and mechanical structures have been performed . Furthermore, the detectors were tested at test beam facilities at CERN and were shown to comply with their design specification.

Three models of the PAMELA apparatus were developed: a mass/thermal model, a technological model for electrical and compatibility tests with the satellite and the flight model for actual data taking in space [51]. All these models were delivered for testing to the TsSKB–Progress factory in Samara, Russia, and shown to be fully compliant with the requirements of the Resurs DK1 spacecraft environment. Specifically, the flight model underwent incoming and acceptance tests in April/May 2005 and was integrated with the satellite in September 2005. Subsequently, PAMELA and the satellite will be transported to Baikonur for the launch into space foreseen for the beginning of 2006.

References

[1] Y. Asaoka et al., Phys. Rev. Lett. 88, 051101 (2002); astro-ph/0109007.
[2] K. Maki, T. Mitsui, T., and S. Orito, Phys. Rev. Lett. 76, 3474 (1996).
[3] L. Bergström, J. Edsjö and P. Ullio, Phys. Rev. D 59, 43506 (1999).
[4] D. Hooper and J. Silk, Phys.Rev. D 71, 083503 (2005).
[5] T. Bringmann, JCAP 0508, 006 (2005); astro-ph/0506219.
[6] M. Aguilar et al., Phys. Rept. 366, 331 (2002).
[7] M. Boezio et al., Astrophys. J. 561, 787 (2001); astro-ph/0103513.
[8] S. Orito et al., Phys. Rev. Lett. 84, 1078 (2000).
[9] G. Basini et al., 26th ICRC, Salt Lake City (1999) 4, 77; see also M. Hof et al., Astrophys. J. 467, L33 (1996).
[10] M. Boezio et al., Astrophys. J. 487, 415 (1997).
[11] J. Mitchell et al., Phys. Rev. Lett. 76, 3057 (1996).
[12] M. Simon, A. Molnar and S. Roesler, Astrophys. J. 499, 250 (1998).
[13] L. Bergström and P. Ullio, private communication (1999).
[14] P. Ullio, astro-ph/9904086 (1999).
[15] R. L. Golden et al., Astron. Astrophys. 188, 145 (1987).
[16] D. Müller and K. K. Tang, Astrophys. J. 312, 183 (1987).
[17] J. M. Clem et al., Astrophys. J. 464, 507 (1996).
[18] R. L. Golden et al., Astrophys. J. 436, 769 (1994).
[19] R. L. Golden et al., Astrophys. J. 457, L103 (1994).
[20] S. W. Barwick et al., Astrophys. J. 498, 779 (1998).
[21] M. Boezio et al., Astrophys. J. 532, 653 (2000); see also G. Barbiellini et al., Astron. Astrophys. 309, L15 (1996).
[22] J. Alcaraz et al., Phys. Lett. B 484, 10 (2000).
[23] M. Boezio et al., Advances in Space Research 27, 669 (2001).
[24] J. J. Beatty et al., Phys. Rev. Lett. 93, 241102 (2004); astro-ph/0412230.
[25] R. J. Protheroe, Astrophys. J. 254, 391 (1982).
[26] I. V. Moskalenko and A. W. Strong, Astrophys. J. 493, 694 (1998).
[27] E. A. Baltz and J. Edsjö, Phys. Rev. D 59, 023511 (1999).
[28] J. Lund, PhD thesis Royal Institute of Technology, Stockholm (2004).
[29] M. Casolino et al., 35^{th} COSPAR Scientific Assembly, Paris (2004), to appear in Advances in Space Research.
[30] A. M. Atoyan, F. A. Aharonian and H. J. Völk, Phys. Rev. D 52, 3265 (1995).
[31] G. Osteria et al., Nucl. Instr. & Meth. A535, 152 (2004).
[32] G. Osteria et al., Nucl. Instr. & Meth. A518, 161 (2004).
[33] G. Osteria et al., Proc. 29th ICRC, Pune, 3, 313 (2005).
[34] S. Orsi et al., Proc. 29th ICRC, Pune, 3, 369 (2005).
[35] J. Lund, "A Study of the PAMELA Anticoincidence System", licentiate thesis Royal Institute of Technology, Stockholm (2002).
[36] S. Orsi et al., "A Second Level Trigger for the PAMELA Satellite Experiment", submitted to Astropart. Phys. (July 2005).
[37] S. Orsi et al., 35^{th} COSPAR Scientific Assembly, Paris (2004), to appear in Advances in Space Research.
[38] O. Adriani et al., Nucl. Instr. & Meth. A 511, 72 (2003).
[39] O. Adriani et al., Proc. 29th ICRC, Pune, 3, 317 (2005).
[40] S. Straulino al., hep-ex/0510012 (2005).
[41] M. Boezio et al., Nucl. Instr. and Meth. A 487, 407 (2002); physics/0109010.

[42] T. Kobayashi et al., 26th ICRC, Salt Lake City (1999), 3, 61.
[43] T. Hebbeker and C. Timmermans, Astropart. Phys. 18, 107 (2002).
[44] M. Motoki et al., Astropart. Phys. 19, 113 (2003).
[45] M. Boezio et al., Phys. Rev. D 67, 072003 (2003).
[46] http://www.be.infn.it/ambriola/gpamela
[47] R. Brun et al., "Detector Description and Simulation Tool", CERN program library (1994).
[48] H. C. Fesefeldt, Technical report PITHA 85-02, Phys. Inst., RWTH Aachen.
[49] J. Lundquist et al., Proc. 29th ICRC, Pune, 3, 305 (2005).
[50] Y. Stozhkov et al., 19^{th} ECRS, Florence (2004), to appear in Int. J. Mod. Phys. A.
[51] R. Sparvoli et al., 35^{th} COSPAR Scientific Assembly, Paris (2004), to appear in Advances in Space Research.